

# Secondary Instability and Mode Jumping of Deep Thermoelastically Buckled Composite Laminates

Hui Chen and Wenbin Yu

*Department of Mechanical and Aerospace Engineering, Utah State University,  
Logan, Utah 84322-4130, USA*

---

## Abstract

An analytic method is presented to study the secondary instability (bifurcation) and mode jumping of thermomechanically deep buckled composite laminates. Unlike most ad hoc approaches, the governing partial differential equations (PDEs) and constitutional relations are derived rigorously from an asymptotically correct, geometrically nonlinear theory. A novel and simpler solution approach is developed to solve the two coupled fourth-order PDEs, namely, the compatibility equation and the dynamic governing equation. The generalized Galerkin method is used to solve boundary value problems corresponding to antisymmetric angle-ply and cross-ply composite plates. The variety of possible modal interactions is expressed in an explicit and concise form by transforming the coupled nonlinear governing equations into a system of nonlinear ordinary differential equations (ODEs).

The comparison between the present method and the finite element analysis (FEA) shows a pretty good match in their numerical results in the primary post-buckling region. While the FEA may lose its convergence when solution comes close to the secondary bifurcation point, the analytic approach has the capability of exploring deeply into the post-secondary buckling realm and capturing the mode jumping phenomenon for various combinations of plate configurations and in-plane boundary conditions. Qualitatively different propagations of buckling pattern are observed before and after mode jumping. Free vibration along the stable primary postbuckling and the jumped equilibrium paths are also studied.

*Key words:* Composite; Laminates; Postbuckling; Mode Jumping; Variational Asymptotic Plate Theory

---

---

*Email address:* [wenbin.yu@usu.edu](mailto:wenbin.yu@usu.edu) (Wenbin Yu).

*URL:* [www.mae.usu.edu/faculty/wenbin](http://www.mae.usu.edu/faculty/wenbin) (Wenbin Yu).

## 1 Introduction

The phenomenon that thin plates under the action of elastic stress may demonstrate a sudden dynamic change of their buckling modes when loaded deeply into the post-buckling regime is often called mode jumping. It has been proven to be of significant importance in explaining various physical observations spreading from mechanics (plate and composite panel deformation [1,2]) to material science (film delamination and thermal barrier coatings [3,4], and heteroepitaxial growth of microelectronic films [5]). A detailed review of recent researches on the secondary instability and dynamic snapping of isotropic plates and shells can be found in [6,7].

Since compressively stressed laminated composite plates and stiffened panels, like their isotropic counterparts, may demonstrate large strength reservations beyond the primary buckling load, numerous experiments and numerical simulations have been conducted to explore the postbuckling response of such structures. Mode jumping of composite structures has been frequently reported in experiments ([8–11], and [2]). However, among the corresponding numerical comparison studies, only computations in the last two papers can successfully predict this phenomenon. Major difficulties can be attribute to the strong geometrical non-linearity demonstrated by the structure when loaded deeply into the postbuckling range and the lack of effective branch switching algorithms to explore the complicated post-secondary buckling equilibria. The first difficulty will induce convergence problems near the secondary bifurcation point or a sharp limit point for most concurrent simulation tools adopting either load incremental or arc-length method [12], while the second is generated by the necessity of tracing through multiple unstable equilibrium segments (blocked by many bifurcation points) which connect two stable equilibrium branches before and after mode jumping [13].

To overcome the branch switching problem, a well known hybrid static/dynamic method is developed by Riks [13] to capture the remote stable branch. In this approach, the dynamic snapping is performed interactively using restarting schemes and dynamic simulating functions available in most finite element packages. However, as indicated in [14], although in many cases this method can successfully predict mode jumping for mechanically loaded structures, it may encounter a spurious convergence problem for thermally stressed plates, where the post-secondary solution converges to an unstable equilibrium branch due to the coupling between the applied external force and the displacement field. The spurious convergence phenomenon can be best illustrated by a recent study of axially compressed composite panels. In this study, a benchmark test of a 4-blade stiffened curved composite panel is conducted by Gemenan Aerospace Center (DLR) and finite element simulations (carried out by using MSC.Nastran, Abaqus/Standard, and LS-Dyna) are performed to compare with the experimental data [10]. The panel is loaded deeply in the postbuckling region and mode jumping is observed at the tertiary bifurcation point in the experiment. In contrast, numerical simulations using various commercial FEA softwares fail to predict the snapping phenomenon, even by applying full dynamic simulations. The simulation results always follow the unstable primary post-buckling branch even though the secondary bifurcation point has already been passed.

An more effective automated hybrid procedure which employs the arc-length method in the quasi-static loading history and a modified dynamic method in the transient phase is presented by Falzon and Cerini to capture the remote stable branch [12]. In [14], a similar

strategy is developed, which uses a non-stationary sweeping scheme capable of adapting large load steps to capture static characteristics of stable equilibrium paths before and after mode jumping and automatically reducing the step size to ensure a dynamic transition between two stable branches. Despite their successes in jumping to the farfield stable states and avoiding spurious convergence, the non-uniqueness of the jumping behavior inherited in any nonlinear system and the possible co-existence of multiple stable branches prevent the two methods to provide a full picture of the mode jumping. To gain a deep insight of mode jumping behavior, an rigorous analytical approach which combines the asymptotically correct, geometrically nonlinear plate theory with the generalized Galerkin's method is develop recently in [15].

With the increasing applications of smart materials (piezoelectric materials, shape memory alloys, and magnetostrictive materials) and functional graded materials in the development of high performance structures, considerable researches have been performed to study the thermal postbuckling behavior of various integrated composite laminated structures.

In [16], the high-order shear deformation theory is combined with a Galerkin-perturbation technique to determine the thermal post-buckling equilibrium. The out-of-plane deformation is assumed to be a single double sine wave. Because of the limitation of the perturbation technique and ignoring mode interactions, solutions obtained by this method is only valid in the vicinity of the primary buckling point. By integrating the higher-order shear deformation theory with a mixed formulation, where inter-layer unknown variables consist of three displacement and three transverse stresses components, thermomechanical postbuckling response of composite laminates is investigated in [17]. Again, the ignorance of nonlinear stain terms in the derivation of stress-displacement relations limits its application to a small initial postbuckling regime. Introducing sufficient mode interaction terms or utilizing finite element method can greatly improve the result's accuracy and broaden its validity to a wilder range in the postbuckling area. Liew et. al. [18] incorporate the first order shear deformation theory with a differential quadrature method to study the thermal postbuckling response of functionally graded laminated composite plates. Although much useful information such as the effects of nonlinear temperature-dependent material properties, layup scheme, and material composition can be obtained, the simulation fails to converge near the secondary buckling point. By constructing a finite element method on the basis of the laywise theory, the snap through scenario is captured during the analysis of thermally buckled shape memory alloy hybrid composite shell panels [19]. However, without stability monitoring, the validity of the occurrence of real jump and the robustness of the algorithm still needs to be verified.

In this paper, mathematically rigorous approach is developed to investigate the secondary instability (bifurcation) and mode jumping of thermomechanically deep buckled metal matrix composite laminates. Kinematic relations and dynamic governing partial differential equations (PDEs) of composite laminates are derived rigorously from an asymptotically correct thermoelastical model. A novel and simpler solution approach is developed to solve the two coupled fourth-order PDEs, namely, the compatibility equation and the dynamic governing equation. Generalized Galerkin method is used to solve boundary value problems corresponding to antisymmetric angle-ply and cross-ply composite plates. Various postbuckling patterns of different complexity are explored before and after the mode jumping. Natural frequencies of the buckled composite plate are calculated along the stable primary postbuckling and the jumped equilibrium paths.

## 2 Asymptotically Correct Geometrically Nonlinear Plate Theory

Many engineering structures made with composite materials have one dimension much smaller than the other two and can be modeled as plates. Plate models are generally derived from three-dimensional (3-D) elasticity theory, making use of the fact that the plate is thin in some sense. Although it is plausible to take into account the smallness of the thickness of such structures, construction of an accurate two-dimensional (2-D) model for a 3-D body still introduces a lot of challenges. One can appreciate this by reading several recent review papers [20–22]. Most of the models that have appeared in the literature, for example [23–26], are based on *ad hoc* kinematic assumptions that cannot be reasonably justified for composite structures, such as an *a priori* distribution of displacement through the thickness.

Mathematically, the approximation in constructing plate models stems from elimination of the thickness coordinate from the original 3-D formulation, a dimensional reduction process inevitably approximate if one wants to take advantage of the smallness of the thickness to simplify the analysis. However, other approximations that are not absolutely necessary should be avoided. For example, for geometrically nonlinear analysis of plates, it is reasonable to assume that the thickness,  $h$ , is small compared to the wavelength of deformation of the reference surface,  $l$ , and the strains are small. Nevertheless, it is not at all reasonable to assume *a priori* some *ad hoc* displacement field, although that is the way most plate theories are constructed.

Hamilton’s extended principle for the dynamics of a 3-D body can be written as:

$$\int_{t_1}^{t_2} \int_v [\delta(\mathcal{K} - \mathcal{F}) + \overline{\delta\mathcal{W}}] dv dt = \overline{\delta\mathcal{A}}, \quad (1)$$

where  $\delta$  is the variation symbol,  $v$  denotes the volume of the undeformed body,  $t_\alpha$  ( $\alpha = 1, 2$ ) are arbitrary fixed times,  $\mathcal{K}$  and  $\mathcal{F}$  are the kinetic and Helmholtz free-energy density, respectively,  $\overline{\delta\mathcal{W}}$  is the virtual work of applied loads, and  $\overline{\delta\mathcal{A}}$  is the virtual action at the boundary of the body. The bars on the last two quantities indicate that they may not be variations of any functionals.

Since in present work we only consider one-way thermechanical coupling and the temperature change due to the deformation of the plate is negligible, we can use the Helmholtz free-energy functional [27] without quadratic terms of temperature to carry out the analysis. This leads to

$$\mathcal{F} = \frac{1}{2} \Gamma^T C \Gamma - \Gamma^T C_\alpha \Delta T, \quad (2)$$

where  $C$  is the  $6 \times 6$  material matrix condensed from the 3-D fourth-order elasticity tensor expressed in the global coordinate system  $x_i$ , ( $i = 1, 2, 3$ ),  $C_\alpha$  a  $6 \times 1$  column matrix representing the 3-D thermal expansion coefficients,  $\Gamma$  denotes the 3-D strain field which are given in [28], and  $\Delta T$  difference of temperature in the structure with respect to the reference temperature when the material is stress free.

To circumvent the difficulty associated with 3-D formulations, we can use the variational asymptotic method [29] to mathematically reduce the 3-D expressions to their two dimensional counterparts as shown in [28] and [30] through an asymptotical expansion of the

variational statements in terms of the following two small parameters:

$$\frac{h}{l} \ll 1 \text{ and } \frac{h}{c\tau} \ll 1, \quad (3)$$

where  $\tau$  is the characteristic scale of change of displacements in time and  $c$  is the minimal velocity of plane waves in the composite material under consideration. The first small parameter is the characteristic of plate and the second small parameter implies that we consider only low-frequency vibrations of composite plates. After the dimensional reduction, the Hamilton's extended principle can be reformulated for the plate reference plane as:

$$\int_{t_1}^{t_2} \int_{\Omega} [\delta(\mathcal{K}_{2D} - \mathcal{F}_{2D}) + \overline{\delta\mathcal{W}}_{2D}] d\Omega dt = \overline{\delta\mathcal{A}}_{2D}, \quad (4)$$

where  $\Omega$  denotes the reference plane,  $\mathcal{K}_{2D}$  and  $\mathcal{F}_{2D}$  are the kinetic energy and Helmholtz free-energy per unit area,  $\overline{\delta\mathcal{W}}_{2D}$  is the virtual work of applied loads, and  $\overline{\delta\mathcal{A}}_{2D}$  is the virtual action at the boundary of plate. Although the theoretical details are given in other papers such as [28,30–32], we listed the final results here for the purpose to be self-contained.

The kinetic energy and the Helmholtz free-energy per unit area are

$$\mathcal{K}_{2D} = \frac{1}{2}\mu(\dot{U}_1^2 + \dot{U}_2^2 + \dot{U}_3^2) \quad (5)$$

$$\mathcal{F}_{2D} = \frac{1}{2} \begin{Bmatrix} \epsilon \\ \kappa \end{Bmatrix}^T \begin{bmatrix} A & B \\ B^T & D \end{bmatrix} \begin{Bmatrix} \epsilon \\ \kappa \end{Bmatrix} - \begin{Bmatrix} \epsilon \\ \kappa \end{Bmatrix}^T \begin{Bmatrix} N_T \\ M_T \end{Bmatrix}, \quad \text{with} \quad (6)$$

$$N_T = \langle A\alpha_e\Delta T \rangle, \quad M_T = \langle x_3A\alpha_e\Delta T \rangle. \quad (7)$$

Here,  $\mu$  is the mass per unit area,  $U_1, U_2, U_3$  the displacements of reference plane in a chosen Cartesian coordinate system,  $\epsilon^T = [\epsilon_{11} \ 2\epsilon_{12} \ \epsilon_{22}]$  the in-plane strains,  $\kappa^T = [\kappa_{11} \ 2\kappa_{12} \ \kappa_{22}]$  the curvatures, and  $\alpha_e^T = [\alpha_{11} \ 2\alpha_{12} \ \alpha_{22}]$  the in-plane thermal expansion coefficients. Dot over the symbol denotes time derivative and angle brackets  $\langle \rangle$  designates the integral throughout the thickness. The  $A, B, D$  matrices and the in-plane thermal stress and momentum resultants  $N_T, M_T$  can be calculated using VAPAS [30,28] and they are the same as those of Classical Lamination Theory if the asymptotical expressions are truncated to the order of  $(h/l)^0$ . It worth mentioning that in this theory no *ad hoc* kinematic assumptions, such as the maintenance of transverse normal line before and after deformations, the infinite rigidity of the transverse normal in the thickness direction, and the negligence of transverse normal stress, have been used during the derivation. The 2-D strain energy in Eq. (7) implies the following definition of plate stress and moment resultants:

$$\begin{Bmatrix} N \\ M \end{Bmatrix} = \begin{bmatrix} A & B \\ B^T & D \end{bmatrix} \begin{Bmatrix} \epsilon \\ \kappa \end{Bmatrix} - \begin{Bmatrix} N_T \\ M_T \end{Bmatrix}, \quad (8)$$

where  $N^T = [N_{11} \ N_{12} \ N_{22}]$  is the vector of in-plane forces per unit length and  $M^T = [M_{11} \ M_{12} \ M_{22}]$  is the vector of bending moments per unit length.

The virtual work done by applied body forces and surface tractions and the virtual action

along the boundary can be listed, respectively, as:

$$\overline{\delta\mathcal{W}}_{2D} = \delta U_1 f_1 + \delta U_2 f_2 + \delta U_3 f_3 + \overline{\delta\psi}_1 m_1 + \overline{\delta\psi}_2 m_2, \quad (9)$$

$$\overline{\delta\mathcal{A}}_{2D} = - \int_{t_1}^{t_2} \int_{\Gamma} (\hat{N}_{\nu\nu} \delta U_{\nu} + \hat{N}_{\nu\tau} \delta U_{\tau} + \hat{N}_{\nu 3} \delta U_3 + \hat{M}_{\nu\nu} \overline{\delta\psi}_{\nu} + \hat{M}_{\nu\tau} \overline{\delta\psi}_{\tau}) d\Gamma dt = 0, \quad (10)$$

where  $f_1, f_2, f_3$  and  $m_1, m_2$  can be calculated from body forces and the applied tractions on boundary surfaces in the modeling process, see [30];  $\overline{\delta\psi}_1, \overline{\delta\psi}_2$  are the virtual rotations. Along the boundary curve  $\Gamma$ , we could specify a force resultant  $\hat{N}_{\nu\nu}$  and a moment resultant  $\hat{M}_{\nu\nu}$  along the outward normal of  $\Gamma$  in the reference plane  $\nu$ ,  $\hat{N}_{\nu\tau}, \hat{M}_{\nu\tau}$  along the tangent of the boundary curve  $\tau$  and  $\hat{N}_{\nu 3}$  along the normal of the reference plane. The virtual quantities  $\delta u_{\nu}, \delta u_{\tau}, \overline{\delta\psi}_{\nu}, \overline{\delta\psi}_{\tau}$  associated with  $\Gamma$  can be calculated from  $\delta u_1, \delta u_2, \overline{\delta\psi}_1, \overline{\delta\psi}_2$  through simple transformations.

It can be shown that Eq. (4) along with Eqs. (5), (7), (9), and (10), provides an approximation of Eq. (1) asymptotically correct up to the order of  $h^0/l^0$  and  $h^0/(c\tau)^0$ . Although this plate theory allows an exact description of geometry, a geometrically-exact theory such as that derived in [31] is unnecessarily overcomplex in studying postbuckling and mode jumping of composite plates. To this end, we specialize the geometrically-exact theory in [31] according to the kinematic assumption that strains are much smaller than the rotations, which is similar to the assumptions used in von Kármán theory for isotropic plates. This assumption helps simplify the expressions for plate strains as

$$\begin{aligned} \epsilon_{11} &= U_{1,1} + \frac{1}{2}U_{3,1}^2, & 2\epsilon_{12} &= U_{1,2} + U_{2,1} + U_{3,1}U_{3,2}, & \epsilon_{22} &= U_{2,2} + \frac{1}{2}U_{3,2}^2, \\ \kappa_{11} &= -U_{3,11}, & \kappa_{12} &= -U_{3,12}, & \kappa_{22} &= -U_{3,22}, \end{aligned} \quad (11)$$

and the virtual rotations can be simply expressed in terms of displacements as

$$\overline{\delta\psi}_1 = -\delta U_{3,1} \quad \overline{\delta\psi}_2 = -\delta U_{3,2}. \quad (12)$$

Aided with these expressions, one can derive the equations of motions from Eq. (4) as

$$\begin{aligned} N_{11,1} + N_{12,2} + f_1 &= \mu \ddot{U}_1, \\ N_{12,1} + N_{22,2} + f_2 &= \mu \ddot{U}_2, \\ M_{11,11} + 2M_{12,12} + M_{22,22} + N_p + f_3 + m_{1,1} + m_{2,2} &= \mu \ddot{U}_3, \end{aligned} \quad (13)$$

with

$$N_p = (N_{11}U_{3,1} + N_{12}U_{3,2})_{,1} + (N_{12}U_{3,1} + N_{22}U_{3,2})_{,2}. \quad (14)$$

The geometry boundary conditions can be trivially specified, and the applied forces and moments associated with the natural boundary conditions on the boundary curve  $\Gamma$  are

$$\begin{aligned} \hat{N}_{\nu\nu} &= n_1^2 N_{11} + 2n_1 n_2 N_{12} + n_2^2 N_{22}, \\ \hat{N}_{\nu\tau} &= n_1 n_2 (N_{22} - N_{11}) + (n_1^2 - n_2^2) N_{12}, \\ \hat{N}_{\nu 3} + \hat{M}_{\nu\tau,\tau} &= (N_{11}U_{3,1} + N_{12}U_{3,2} + M_{11,1} + M_{12,2})n_1, \\ &\quad + (N_{12}U_{3,1} + N_{22}U_{3,2} + M_{12,1} + M_{22,2})n_2 + m_1 n_1 + m_2 n_2 + M_{\nu\tau,\tau}, \\ \hat{M}_{\nu\nu} &= M_{\nu\nu}, \end{aligned} \quad (15)$$

where  $n_1 = \cos \phi$ ,  $n_2 = \sin \phi$ ,  $\phi$  is the angle between the outward normal of the boundary and  $x_1$  direction, and

$$M_{\nu\nu} = n_1^2 M_{11} + 2n_1 n_2 M_{12} + n_2^2 M_{22}, \quad M_{\nu\tau} = n_1 n_2 (M_{22} - M_{11}) + (n_1^2 - n_2^2) M_{12}. \quad (16)$$

Of course, as it is known in the classical plate theory, conditions for concentrated forces at the corners of the plate boundary conditions will appear as follows

$$(M_{\nu\tau} - \hat{M}_{\nu\tau})_{i^+} - (M_{\nu\tau} - \hat{M}_{\nu\tau})_{i^-} = R_i \quad (17)$$

with  $R_i$  are the concentrated forces at the  $i$ th corner,  $i^+$  denotes evaluation at the left end of the corner and  $i^-$  denotes evaluation at the right end of the corner.

### 3 Analytic Solutions

One goal of the present work is to seek analytic solutions for this asymptotically correct, geometrically nonlinear composite plate theory, particularly for the postbuckling and mode jumping analysis due to temperature changes. To this end, we only focus on thermomechanically stressed simply-supported rectangular plates without in-plane distributed loads and momenta,  $f_1 = f_2 = m_1 = m_2 = 0$ , and considering the in-plane velocities,  $\ddot{U}_1$  and  $\ddot{U}_2$ , negligible in comparison to  $\ddot{U}_3$ . The plate under investigation is sketched in Fig. 1, where the temperature field is assumed to be a function of  $x_3$ , i.e.,  $\Delta T = \Delta T(x_3)$ . For illustrative purpose, we provide detailed formulations for antisymmetric angle-ply and cross-ply laminates. As it will be clear in the following derivation, the method developed in this paper actually provides a general way to deal with both in-plane and out-of-plane boundary conditions and can be readily extended to analyzing composite plates with arbitrary lamination scheme.

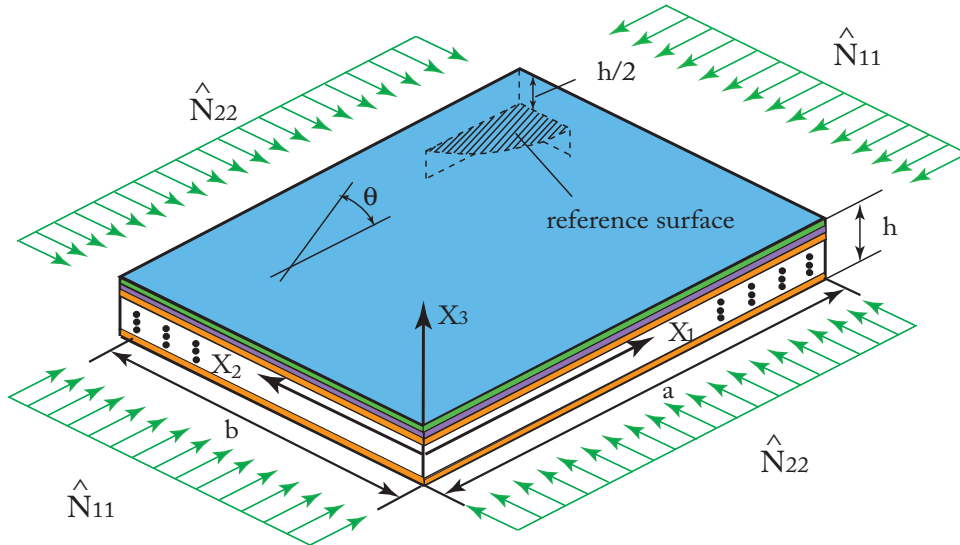


Fig. 1. Schematic of laminated plates

### 3.1 Governing differential equations for laminated composite plates

With the constitutive relations for the laminated composite plate obtained in Eq. (8), its partial inverse takes the form of

$$\begin{Bmatrix} \varepsilon \\ M \end{Bmatrix} = \begin{bmatrix} A^* & B^* \\ H^* & D^* \end{bmatrix} \begin{Bmatrix} N \\ \kappa \end{Bmatrix} + \begin{Bmatrix} \epsilon_T \\ \mathfrak{M}_T \end{Bmatrix}, \quad (18)$$

where,  $A^* = A^{-1}$ ,  $B^* = -A^{-1}B$ ,  $H^* = -B^{*T}$ ,  $D^* = D - B^T A^{-1}B$ ,  $\epsilon_T = A^* N_T$ , and  $\mathfrak{M}_T = -B^{*T} N_T - M_T$ .

By introducing an Airy stress function defined by:

$$N_{11} = F_{,22}, \quad N_{12} = -F_{,12}, \quad \text{and} \quad N_{22} = F_{,11},$$

one can derive the von Kámán compatibility equation for generalized composite laminated plates from the first three equations of Eq. (11) as

$$\begin{aligned} & A_{22}^* F_{,1111} + (2A_{12}^* + A_{66}^*) F_{,1122} + A_{11}^* F_{,2222} - 2A_{26}^* F_{,1112} - 2A_{16}^* F_{,1222} = \\ & U_{3,12}^2 - U_{3,11} U_{3,22} + B_{21}^* U_{3,1111} + (B_{11}^* - 2B_{66}^* + B_{22}^*) U_{3,1122} + B_{12}^* U_{3,2222} \quad (19) \\ & + (2B_{26}^* - B_{61}^*) U_{3,1112} + (2B_{16}^* - B_{62}^*) U_{3,1222}. \end{aligned}$$

One can easily check that the Airy stress function automatically satisfy the first two equations of motions in Eq. (13) with aforementioned specialization and assumptions. The last equation in Eq. (13) can now be rewritten as

$$\begin{aligned} & \mu \ddot{U}_3 + D_{11}^* U_{3,1111} + 2(D_{12}^* + 2D_{66}^*) U_{3,1122} + D_{22}^* U_{3,2222} + 4D_{16}^* U_{3,1112} \\ & + 4D_{26}^* U_{3,1222} + B_{21}^* F_{,1111} + (B_{11}^* - 2B_{66}^* + B_{22}^*) F_{,1122} \quad (20) \\ & + B_{12}^* F_{,2222} + (2B_{26}^* - B_{61}^*) F_{,1112} + (2B_{16}^* - B_{62}^*) F_{,1222} \\ & = f_3 + F_{,22} U_{3,11} - 2F_{,12} U_{3,12} + F_{,11} U_{3,22}, \end{aligned}$$

where  $f_3$  denotes total transverse load per unit. Therefore, by assuming the temperature distribution  $\Delta T(x_3)$  being independent of  $x_1$  and  $x_2$ , the two equations (19) and (20) take the same form as those of the mechanically compressed composite laminates [15].

It noted that the significant difference of the order of the magnitudes of coefficients in above dimensional PDEs may cause convergence problem when tracing the postbuckling paths through bifurcation points. This can be avoided by introducing the following dimensionless quantities (indicated by a tilde):

$$\begin{aligned} \tilde{x}_1 &= \frac{x_1}{a}, & \tilde{x}_2 &= \frac{x_2}{a}, & \tilde{U}_3 &= \frac{U_3}{\sqrt{A_{22}^* D_{11}^*}}, & r &= b/a, \quad (21) \\ \tilde{F} &= \frac{F}{D_{11}^*}, & \tilde{q}_t &= \frac{a^4 f_3}{D_{11}^* \sqrt{D_{11}^* A_{22}^*}}, & \tau &= \sqrt{\frac{D_{11}^*}{a^4 \mu}} t, \end{aligned}$$

where  $r$  is the aspect ratio of the plate and  $\tau$  denotes the non-dimensional time. The dimen-

sionless compatibility and governing equations now takes the form of

$$\begin{aligned} & \tilde{A}_{22}\tilde{F}_{,1111} + (2\tilde{A}_{12} + \tilde{A}_{66})\tilde{F}_{,11\bar{2}\bar{2}} + \tilde{A}_{11}\tilde{F}_{,\bar{2}\bar{2}\bar{2}\bar{2}} - 2\tilde{A}_{26}\tilde{F}_{,11\bar{1}\bar{2}} - 2\tilde{A}_{16}\tilde{F}_{,\bar{1}\bar{2}\bar{2}\bar{2}} = \\ & \tilde{U}_{3,\bar{1}\bar{2}}^2 - \tilde{U}_{3,\bar{1}\bar{1}}\tilde{U}_{3,\bar{2}\bar{2}} + \tilde{B}_{21}\tilde{U}_{3,1111} + (\tilde{B}_{11} - 2\tilde{B}_{66} + \tilde{B}_{22})\tilde{U}_{3,11\bar{2}\bar{2}} + \tilde{B}_{\bar{1}\bar{2}}\tilde{U}_{3,\bar{2}\bar{2}\bar{2}\bar{2}} \\ & + (2\tilde{B}_{26} - \tilde{B}_{61})\tilde{U}_{3,11\bar{1}\bar{2}} + (2\tilde{B}_{16} - \tilde{B}_{62})\tilde{U}_{3,\bar{1}\bar{2}\bar{2}\bar{2}}, \end{aligned} \quad (22)$$

and

$$\begin{aligned} & \tilde{U}_3'' + \tilde{D}_{11}\tilde{U}_{3,1111} + 2(\tilde{D}_{12} + 2\tilde{D}_{66})\tilde{U}_{3,11\bar{2}\bar{2}} + \tilde{D}_{22}\tilde{U}_{3,\bar{2}\bar{2}\bar{2}\bar{2}} + 4\tilde{D}_{16}\tilde{U}_{3,11\bar{1}\bar{2}} \\ & + 4\tilde{D}_{26}\tilde{U}_{3,\bar{1}\bar{2}\bar{2}\bar{2}} + \tilde{B}_{21}\tilde{F}_{,1111} + (\tilde{B}_{11} - 2\tilde{B}_{66} + \tilde{B}_{22})\tilde{F}_{,11\bar{2}\bar{2}} \\ & + \tilde{B}_{12}\tilde{F}_{,\bar{2}\bar{2}\bar{2}\bar{2}} + (2\tilde{B}_{26} - \tilde{B}_{61})\tilde{F}_{,11\bar{1}\bar{2}} + (2\tilde{B}_{16} - \tilde{B}_{62})\tilde{F}_{,\bar{1}\bar{2}\bar{2}\bar{2}} \\ & = \tilde{q}_t + \tilde{F}_{,\bar{2}\bar{2}}\tilde{U}_{3,11} - 2\tilde{F}_{,\bar{1}\bar{2}}\tilde{U}_{3,\bar{1}\bar{2}} + \tilde{F}_{,\bar{1}\bar{1}}\tilde{U}_{3,\bar{2}\bar{2}}, \end{aligned} \quad (23)$$

where  $()'' = \partial^2()/\partial\tau^2$ ,  $\tilde{A} = 1/A_{22}^*A^*$ ,  $\tilde{B} = 1/\sqrt{A_{22}^*D_{11}^*}B^*$ , and  $\tilde{D} = 1/D_{11}^*D^*$ .

With the further introduction of the following additional dimensionless relations,

$$\begin{aligned} \tilde{U}_1 &= \frac{a}{A_{22}^*D_{11}^*}U_1, & \tilde{U}_2 &= \frac{a}{A_{22}^*D_{11}^*}U_2, & (\tilde{\varepsilon}, \tilde{\varepsilon}_T) &= \frac{a^2}{A_{22}^*D_{11}^*}(\varepsilon, \varepsilon_T), \\ \tilde{\kappa} &= \frac{a^2}{\sqrt{A_{22}^*D_{11}^*}}\kappa, & (\tilde{N}, \tilde{N}_T) &= \frac{a^2}{D_{11}^*}(N, N_T), & (\tilde{M}, \tilde{M}_T) &= \frac{a^2}{D_{11}^*\sqrt{A_{22}^*D_{11}^*}}(M, M_T), \\ \tilde{A}_A &= A_{22}^*A, & \tilde{B}_B &= \frac{A_{22}^*}{\sqrt{A_{22}^*D_{11}^*}}B, & \tilde{D}_D &= \frac{1}{D_{11}^*}D, \end{aligned} \quad (24)$$

all the previously derived physical relations, such as kinematic relations in Eqs. (11) and (12) and constitutive laws in Eqs. (8) and (18) still hold their original formats, no unnecessary changes are needed. Thus, by carefully selecting the nondimensionalization scheme, not only can the equation coefficients be re-scaled to the same order, but also their physical meanings could be retained.

For simplicity, except for such dimensionless coefficients as in  $\tilde{A}$ ,  $\tilde{B}$ , and  $\tilde{D}$  matrices, we use the dimensionless values and drop the tilde throughout the rest of the paper.

### 3.2 Boundary conditions

In order to describe in-plane boundary conditions, the in-plane forces,  $\hat{N}_{11}$ ,  $\hat{N}_{22}$ , applied along the plate edges are each partitioned into two parts: the uniformly distributed forces,  $\bar{N}_{11}$  or  $\bar{N}_{22}$ , and the variational one,  $F_{,22}^p(x_1, x_2)$  or  $F_{,11}^p(x_1, x_2)$ , *i.e.*,

$$\hat{N}_{11} = \bar{N}_{11} + F_{,22}^p(x_1, x_2), \quad \hat{N}_{22} = \bar{N}_{22} + F_{,11}^p(x_1, x_2), \quad (25)$$

where  $F^p(x_1, x_2)$  is the particular solution of the compatibility equation and explicit expressions will be given in the next subsection for specific cases.

Two types of boundary conditions are usually considered dealing with buckling and postbuckling analysis, namely, the straight-edge (constant end shortening) one (26) and the in-plane

fixed one (27):

$$\begin{aligned} U_3 = \hat{N}_{12} = \hat{M}_{11} = 0, U_1 = \text{constant}, & \quad \text{at } x_1 = 0, 1, \\ U_3 = \hat{N}_{12} = \hat{M}_{22} = 0, U_2 = \text{constant}, & \quad \text{at } x_2 = 0, r, \end{aligned} \quad (26)$$

$$\begin{aligned} U_1 = U_2 = U_3 = 0, M_{11} = 0, & \quad \text{at } x_1 = 0, 1, \\ U_1 = U_2 = U_3 = 0, M_{22} = 0, & \quad \text{at } x_2 = 0, r. \end{aligned} \quad (27)$$

It is clear by setting the constant in (26) equal to zero, one gets the zero-end-shortening boundary condition. In the present study, without loss of generality, we will apply the straight-edge boundary condition for antisymmetric angle-ply laminates and the in-plane fixed one for cross-ply laminates.

### 3.3 Transformation to nonlinear ODEs

Now, the objective of our nonlinear analysis becomes solving the two coupled partial differential equations (PDEs), Eqs. (22) and (23), subjected to boundary conditions in either Eq. (26) or Eq. (27). This certainly is not a trivial problem, especially for seeking analytic solutions. We will rely on Fourier series expansion to transform the PDEs into ordinary differential equations (ODEs), which is illustrated for both antisymmetric angle-ply and cross-ply laminates as follows.

#### 3.3.1 Angle-ply laminates

For antisymmetric angle-ply laminated plates, some components in  $\tilde{A}$ ,  $\tilde{B}$ , and  $\tilde{D}$  are always zero, therefore, the compatibility equation and the governing equation in Eqs. (22) and (23) can be simplified as:

$$\begin{aligned} \tilde{A}_{22}F_{,1111} + (2\tilde{A}_{12} + \tilde{A}_{66})F_{,1122} + \tilde{A}_{11}F_{,2222} = \\ U_{3,12}^2 - U_{3,11}U_{3,22} + (2\tilde{B}_{26} - \tilde{B}_{61})U_{3,1112} + (2\tilde{B}_{16} - \tilde{B}_{62})U_{3,1222}, \end{aligned} \quad (28)$$

$$\begin{aligned} U_3'' + \tilde{D}_{11}U_{3,1111} + 2(\tilde{D}_{12} + 2\tilde{D}_{66})U_{3,1122} + \tilde{D}_{22}U_{3,2222} + (2\tilde{B}_{26} - \tilde{B}_{61})F_{,1112} \\ + (2\tilde{B}_{16} - \tilde{B}_{62})F_{,1222} = f_3 + F_{,22}U_{3,11} - 2F_{,12}U_{3,12} + F_{,11}U_{3,22}. \end{aligned} \quad (29)$$

For a simply-supported laminated plate, the transverse deflection  $w$  can be expressed as double Fourier series:

$$U_3 = \sum_{k,l} W_{kl} \sin k\pi x_1 \sin \frac{l\pi x_2}{r}, \quad (30)$$

where  $W_{kl}$  represents the amplitude of the buckling mode with  $k$  and  $l$  half-waves over the longitudinal and the lateral directions; odd values of the subscripts  $k$  and  $l$  denote symmetric modes while even values denote the antisymmetric ones.

Using the Fourier expansion in Eq. (30), one can transform the two coupled spatial-temporal PDEs to a system of nonlinear ODEs governing the modal amplitude. To achieve this, we need to deal with the compatibility equation first. In view of Eq. (25), we assume that the solution of Eq. (28) also contains a homogeneous solution  $F^h(x_1, x_2)$  and a particular solution  $F^p(x_1, x_2)$ , such that

$$F(x_1, x_2) = F^h(x_1, x_2) + F^p(x_1, x_2), \quad (31)$$

with

$$F^h(x_1, x_2) = -\frac{1}{2}\bar{N}_{11}x_2^2 - \frac{1}{2}\bar{N}_{22}x_1^2. \quad (32)$$

Substituting Eq. (30) into Eq. (28) and carrying out some algebraic and calculus operations yield the particular solution of the compatibility equation:

$$F^p(x_1, x_2) = \left(\frac{r^2}{4}\right) \sum_{k,l,m,n} W_{kl}W_{mn}S_{1x}^T C_{klmn}S_{1y} + \sum_{k,l} W_{kl}c_{5kl} \cos(k\pi x_1) \cos\left(\frac{l\pi x_2}{r}\right), \quad (33)$$

where,

$$S_{1x} = \begin{Bmatrix} \cos((k+m)\pi x_1) \\ \cos((k-m)\pi x_1) \end{Bmatrix}, \quad C_{klmn} = \begin{bmatrix} c_1 & c_2 \\ c_3 & c_4 \end{bmatrix}, \quad S_{1y} = \begin{Bmatrix} \cos\left(\frac{(l+n)\pi x_2}{r}\right) \\ \cos\left(\frac{(l-n)\pi x_2}{r}\right) \end{Bmatrix}. \quad (34)$$

The coefficients  $c_1 \sim c_4$  in matrix  $C_{klmn}$  and  $c_{5kl}$  are given by

$$\begin{aligned} c_1 &= \frac{klmn - k^2n^2}{\tilde{A}_{22}(k+m)^4r^4 + (2\tilde{A}_{12} + \tilde{A}_{66})r^2(k+m)^2(l+n)^2 + \tilde{A}_{11}(l+n)^4} \\ c_2 &= \frac{klmn + k^2n^2}{\tilde{A}_{22}(k+m)^4r^4 + (2\tilde{A}_{12} + \tilde{A}_{66})r^2(k+m)^2(l-n)^2 + \tilde{A}_{11}(l-n)^4} \\ c_3 &= \frac{klmn + k^2n^2}{\tilde{A}_{22}(k-m)^4r^4 + (2\tilde{A}_{12} + \tilde{A}_{66})r^2(k-m)^2(l+n)^2 + \tilde{A}_{11}(l+n)^4} \\ c_4 &= \frac{klmn - k^2n^2}{\tilde{A}_{22}(k-m)^4r^4 + (2\tilde{A}_{12} + \tilde{A}_{66})r^2(k-m)^2(l-n)^2 + \tilde{A}_{11}(l-n)^4} \\ c_{5kl} &= \frac{klr [(\tilde{B}_{61} - 2\tilde{B}_{26})k^2r^2 + (\tilde{B}_{62} - 2\tilde{B}_{16})l^2]}{\tilde{A}_{22}k^4r^4 + (2\tilde{A}_{12} + \tilde{A}_{66})(rkl)^2 + \tilde{A}_{11}l^4}, \end{aligned} \quad (35)$$

where  $c_4 = 0$  if  $k = m$  and  $l = n$ .

It is easy to verify that the solution  $F(x_1, x_2)$  automatically satisfies the zero shear force and zero momentum boundary conditions along edges expressed in Eq. (26). Resorting to (18), one can show that zero momentum requirements in (26) is satisfied for thermomechanically loading cases with uniformly distributed temperature field. Next, by following end shortening definitions expressed as

$$\begin{aligned} \Delta_{11} &= \int_0^1 U_{1,1}dx_1 = \int_0^1 (\varepsilon_{11} - \frac{1}{2}U_{3,1}^2)dx_1 \quad (\text{end shortening along } x_1 \text{ direction}), \\ \Delta_{22} &= \int_0^r U_{2,2}dx_2 = \int_0^r (\varepsilon_{22} - \frac{1}{2}U_{3,2}^2)dx_2 \quad (\text{end shortening along } x_2 \text{ direction}), \end{aligned} \quad (36)$$

one can prove that the straight-edge boundary conditions are also satisfied. The constant end shortenings take the form of:

$$\Delta_{11} = -\left(\frac{\pi^2}{8}\right) \sum_{k,l} W_{kl}^2 k^2 - (\tilde{A}_{11}\bar{N}_{11} + \tilde{A}_{12}\bar{N}_{22}) + \Delta_{T11}, \quad (37)$$

$$\Delta_{22} = - \left( \frac{\pi^2}{8r} \right) \sum_{k,l} W_{kl}^2 l^2 - r \left( \tilde{A}_{12} \bar{N}_{11} + \tilde{A}_{22} \bar{N}_{22} \right) + \Delta_{T22}, \quad (38)$$

with  $\Delta_{T11} = \int_0^1 \epsilon_{T11} dx_1$  and  $\Delta_{T22} = \int_0^r \epsilon_{T22} dx_2$  representing end shortenings caused by the thermal effect.  $\Delta_{T11}$  and  $\Delta_{T22}$  are constants if the temperature field do not depend on  $x_1$  and  $x_2$ .

Finally, the dynamic governing equation in Eq.(29) can be transformed to a series of nonlinear ODEs with respect to the modal amplitudes  $W_{kl}$  by using a generalized Galerkin procedure with a weighting function  $\phi_{pq}(x_1, x_2)$  with the form of

$$\phi_{pq}(x_1, x_2) = \sin(p\pi x_1) \sin\left(\frac{q\pi x_2}{r}\right). \quad (39)$$

By letting

$$\begin{aligned} f_u &= \tilde{D}_{11} U_{3,1111} + 2(\tilde{D}_{12} + 2\tilde{D}_{66}) U_{3,1122} + \tilde{D}_{22} U_{3,2222}, \\ f_F &= (2\tilde{B}_{26} - \tilde{B}_{61}) F_{,1112} + (2\tilde{B}_{16} - \tilde{B}_{62}) F_{,1222}, \\ f_{F_u} &= F_{,22} U_{3,11} - 2F_{,12} U_{3,12} + F_{,11} U_{3,22} \end{aligned} \quad (40)$$

and defining the inner product of two arbitrary functions of  $f(x_1, x_2)$  and  $g(x_1, x_2)$  as

$$[f(x_1, x_2), g(x_1, x_2)] \stackrel{\text{def}}{=} \int_0^a \int_0^b f(x_1, x_2) g(x_1, x_2) dx_1 dx_2, \quad (41)$$

we can transform the dynamic governing equation in Eq. (29) to be

$$[U_3'', \phi_{pq}] + [f_u, \phi_{pq}] + [f_F, \phi_{pq}] = [f_3, \phi_{pq}] + [f_{F_u}, \phi_{pq}] + \int_{\Gamma_\sigma} (M_{nn} - \hat{M}_{nn}) \frac{\partial \delta \phi_{pq}}{\partial n} ds. \quad (42)$$

Here, the last integral term takes account of non-zero boundary effects. Substituting expressions for  $U_3$  and  $F$  defined in Eqs. (30), (31), (32), and (33) into the above equation and performing some linear algebraic operations lead to a successful transformation of the two coupled PDEs in Eqs.(28) and (29) into a compactly formulated series of nonlinear ODEs expressed explicitly in terms of amplitudes of corresponding buckling mode as:

$$\begin{aligned} W_{pq}'' + \left(\frac{\pi}{r}\right)^4 & \left\{ [\tilde{D}_{11}(pr)^4 + 2(\tilde{D}_{12} + 2\tilde{D}_{66})(rpq)^2 + \tilde{D}_{22}q^4] \right. \\ & \left. - c_{5pq} r p q [(2\tilde{B}_{26} - \tilde{B}_{61})(pr)^2 + (2\tilde{B}_{16} - \tilde{B}_{62})q^2] - \left(\frac{r}{\pi}\right)^2 [\bar{N}_{11}(pr)^2 + \bar{N}_{22}q^2] \right\} W_{pq} \\ & = \left(\frac{4}{r}\right) [f_3, \phi_{pq}] + \left(\frac{\pi^4}{r^2}\right) \sum_{k,l,m,n} W_{kl} W_{mn} V_{1x}^T (rL_1 + c_{5mn}G_1) V_{1y} \\ & + \left(\frac{\pi^4}{4}\right) \sum_{i,j,k,l,m,n} W_{ij} W_{kl} W_{mn} V_{2x}^T E V_{2y} + g(\Delta T), \end{aligned} \quad (43)$$

where, the coefficient  $g(\Delta T)$ , vectors  $V_{1x}$ ,  $V_{1y}$ ,  $V_{2x}$ ,  $V_{2y}$ , and matrices  $G_1$ ,  $L_1$ ,  $E$  are provided in Appendix A.

The inner product of the transverse load and the Galerkin's weighting function  $[f_3, \phi_{pq}]$  takes the form of either  $q_0 \sin(p\pi x_{10}) \sin(q\pi x_{20}/r)$  or  $4q_0 r / (pq\pi^2)$  for  $p, q = 1, 3, 5, \dots$ , depending on whether the vertical load is concentrated or uniformly distributed.

### 3.3.2 Cross-ply laminates

For antisymmetric cross-ply laminated plates, zeroes existing in  $\tilde{A}$ ,  $\tilde{B}$ , and  $\tilde{D}$  enable us to simplify the compatibility equation and the governing equation in Eqs. (22) and (23) as:

$$\begin{aligned} \tilde{A}_{22}F_{,1111} + (2\tilde{A}_{12} + \tilde{A}_{66})F_{,1122} + \tilde{A}_{11}F_{,2222} = \\ U_{3,12}^2 - U_{3,11}U_{3,22} + \tilde{B}_{21}U_{3,1111} + (\tilde{B}_{11} + \tilde{B}_{22})U_{3,1122} + \tilde{B}_{12}U_{3,2222}, \end{aligned} \quad (44)$$

$$\begin{aligned} U_3'' + \tilde{D}_{11}U_{3,1111} + 2(\tilde{D}_{12} + 2\tilde{D}_{66})U_{3,1122} + \tilde{D}_{22}U_{3,2222} + \tilde{B}_{21}F_{,1111} \\ + (\tilde{B}_{11} + \tilde{B}_{22})F_{,1122} + \tilde{B}_{12}F_{,2222} = f_3 + F_{,22}U_{3,11} - 2F_{,12}U_{3,12} + F_{,11}U_{3,22}. \end{aligned} \quad (45)$$

Similar to the analysis of antisymmetric angle-ply laminates, the general solution of the compatibility equation can be expressed as

$$\begin{aligned} F(x_1, x_2) = -\frac{1}{2}\bar{N}_{11}x_2^2 - \frac{1}{2}\bar{N}_{22}x_1^2 + \left(\frac{r^2}{4}\right) \sum_{k,l,m,n} W_{kl}W_{mn}S_{1x}^T C_{klmn}S_{1y} \\ + \sum_{k,l} W_{kl} c_{6kl} \sin(k\pi x_1) \sin\left(\frac{l\pi x_2}{r}\right), \end{aligned} \quad (46)$$

with coefficients  $c_1, c_2, c_3, c_4$  given by Eq. (35) and  $c_{6kl}$  given by

$$c_{6kl} = \frac{\tilde{B}_{21}(kr)^4 + (\tilde{B}_{11} + \tilde{B}_{22})(klr)^2 + \tilde{B}_{12}l^4}{\tilde{A}_{22}(kr)^4 + (2\tilde{A}_{12} + \tilde{A}_{66})(klr)^2 + \tilde{A}_{11}l^4}. \quad (47)$$

The end shortenings along the  $x_1$  and  $x_2$  directions now become

$$\begin{aligned} \Delta_{11} = \Delta_{T11} - (\bar{N}_{11}\tilde{A}_{11} + \bar{N}_{22}\tilde{A}_{12}) - \left(\frac{\pi^2}{8}\right) \sum_{k,l} W_{kl}^2 k^2 \\ - \left(\frac{2\pi}{r^2}\right) \sum_{\substack{k,l \\ k=1,3,5,\dots}} W_{kl} \frac{(c_{6kl}\tilde{A}_{12} - \tilde{B}_{11})(kr)^2 + (c_{6kl}\tilde{A}_{11} - \tilde{B}_{12})l^2}{k} \sin\left(\frac{l\pi x_2}{r}\right), \end{aligned} \quad (48)$$

$$\begin{aligned} \Delta_{22} = \Delta_{T22} - (\bar{N}_{11}\tilde{A}_{12} + \bar{N}_{22}\tilde{A}_{22})r - \left(\frac{\pi^2}{8r}\right) \sum_{k,l} W_{kl}^2 l^2 \\ - \left(\frac{2\pi}{r}\right) \sum_{\substack{k,l \\ l=1,3,5,\dots}} W_{kl} \frac{(c_{6kl}\tilde{A}_{22} - \tilde{B}_{21})(kr)^2 + (c_{6kl}\tilde{A}_{12} - \tilde{B}_{22})l^2}{l} \sin(k\pi x_1). \end{aligned} \quad (49)$$

Clearly, the end shortening terms are no-longer constants. Moreover, even under pure mechanical loadings, the general solution obtained above satisfies neither the zero resultant moment nor the zero shear force requirement on boundaries, indicating the typical prebuckling deformation behavior characterized by antisymmetric cross-ply laminates.

By changing the definition of  $f_F$  in Eq. (40) to

$$f_F = \tilde{B}_{21}F_{,1111} + (\tilde{B}_{11} + \tilde{B}_{22})F_{,1122} + \tilde{B}_{12}F_{,2222} \quad (50)$$

and applying the generalized Galerkin method to Eq. (45), the dynamic governing equation for cross-ply laminates becomes

$$\begin{aligned}
[U_3'', \phi_{pq}] + [f_u, \phi_{pq}] + [f_F, \phi_{pq}] &= [f_3, \phi_{pq}] + [f_{Fu}, \phi_{pq}] + \int_{\Gamma_\sigma} M_{nn} \frac{\partial \phi_{pq}}{\partial n} ds. \\
- \int_{\Gamma_\sigma} [(N_{nn} - (-\bar{N}_{nn})) \delta U_n + (N_{ns} - (-\bar{N}_{ns})) \delta U_s] ds,
\end{aligned} \tag{51}$$

where, the first integration term represents the boundary effect of the bending moment while the last integration the in-plane force boundary effects.

For simplicity, in-plane fixed boundary condition in Eq. (27) is considered for plate with this kind of lamination configuration. More generalized boundary cases such as the specification of boundary forces have been consider by the authors in [15]. The final form of the dynamic governing equation is therefore given by

$$\begin{aligned}
W_{pq}'' - \left(\frac{4}{r}\right) (C_{B1}\bar{N}_{11} + C_{B2}\bar{N}_{22}) + \left(\frac{\pi}{r}\right)^4 \{ & [\tilde{D}_{11}(pr)^4 + 2(\tilde{D}_{12} + 2\tilde{D}_{66})(pqr)^2 + \tilde{D}_{22}q^4] \\
+ c_{6pq} [\tilde{B}_{21}(pr)^4 + (\tilde{B}_{11} + \tilde{B}_{22})(pqr)^2 + \tilde{B}_{12}q^4] - \left(\frac{r}{\pi}\right)^2 & (\bar{N}_{11}(pr)^2 + \bar{N}_{22}q^2) \} W_{pq} \\
= \left(\frac{4}{r}\right) [f_3, \phi_{pq}] + \frac{\pi^4}{4} \sum_{i,j,k,l,m,n} W_{ij}W_{kl}W_{mn}V_{2x}^T E V_{2y} & \\
+ \left(\frac{\pi^2}{4r^2}\right) \sum_{k,l,m,n} W_{kl}W_{mn} \left[ V_{3x}^T (c_{6mn}G_2 - L_2) V_{3y} + \left(\frac{16r}{\pi^2}\right) C_{L3} V_{4x}^T L_3 V_{4y} \right] & + g(\Delta T),
\end{aligned} \tag{52}$$

where, coefficients  $C_{B1}$ ,  $C_{B2}$ ,  $C_{L3}$ , vectors  $V_{3x}$ ,  $V_{4x}$ ,  $V_{3y}$ ,  $V_{4y}^T$ , and matrices  $G_2$ ,  $L_2$ ,  $L_3$  are provided in Appendix A. Under the in-plan fixed boundary condition, the in-plane force boundary effect automatically vanishes.

### 3.4 Postbuckling analysis

For postbuckling analysis, we need to rewrite the amplitude equations presented in dynamic equations Eq. (43) and Eq. (52) in matrix form as

$$M\ddot{W} + K_w W = f(W, \bar{N}_{11}, \bar{N}_{22}), \tag{53}$$

where  $W$  consists of amplitudes of the assumed buckling modes,  $M$  and  $K_w$  represent the corresponding mass and stiffness matrices, and  $f(W, \bar{N}_{11}, \bar{N}_{22})$  denotes nonlinear terms. It is obvious that the dimensionless diagonal mass matrix  $M = I$  is positive definite. Hence the dynamic stability (in the Lyapunov sense) of the equilibrium paths is determined by the sign of the smallest eigenvalue of the stiffness matrix  $K_w$ .

Parametric continuation method is used to obtained the stationary solution of the nonlinear ODEs in Eq. (53) and the stability of the equilibrium paths are determined by the positive definiteness of the stiffness matrix. A continuation package— AUTO [33] is used to follow the equilibrium path and log the bifurcation points. Natural frequencies of small amplitude free vibrations along stable equilibrium paths (before and after mode jumping) are calculated by locally linearizing the nonlinear dynamic system and solving the associated eigenvalue

problem. By this we can trace the characteristics of the free vibration of the composite plate before and after mode jumping.

## 4 Results and Discussions

In this section, the outlined method is verified by comparing its results with those obtained through FEA using a commercial package ANSYS. Then, we will apply the developed method to analyze the thermomechanical behaviors of the secondary instability and mode jumping for both antisymmetric angle-ply and cross-ply laminated plates with four edges simply-supported out of plane.

### 4.1 Static analysis

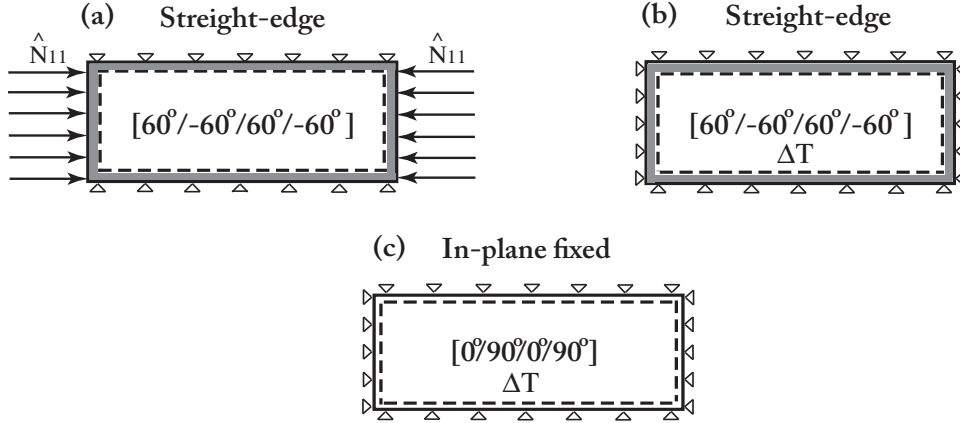


Fig. 2. Sketches of three cases investigated. (a) case 1: thermomechanically loaded angle-ply laminated plate, straight-edge, two unloaded edges in-plane constrained; (b) case 2: thermally loaded angle-ply laminated plate, straight-edge, four edges in-plane constrained; (c) case 3: thermally loaded cross-ply laminated plate, four edges in-plane fixed.

As illustrated in Fig. 2, in present work we will investigate the following three cases:

- case 1: a thermal mechanically loaded  $[60^\circ / -60^\circ / 60^\circ / -60^\circ]$  plate, with constant end shortening along  $x_1$  direction and two unloaded edges remaining straight and constrained in-plane; see Eq. (26) and Fig. 2 (a).
- case 2: a thermally loaded  $[60^\circ / -60^\circ / 60^\circ / -60^\circ]$  plate, with four edges remaining straight and constrained in-plane; see Eq. (26) and Fig. 2 (b).
- case 3: a thermally loaded  $[90^\circ / 0^\circ / 90^\circ / 0^\circ]$  plate with four edges fixed in-plane; see Eq. (27) and Fig. 2 (c).

For all these three cases, the aspect ratio of the laminated plate is set as  $a/b = 2.5$  and side-to-thickness ratio is selected as  $b/h = 75$  to represent thin composite plates. Although the present method can use dimensionless parameters to simplify the analysis of a group of practical problems with a single computational process, to facilitate the comparison with ANSYS, we chose  $a = 1.5 \text{ m}$ ,  $b = 0.6 \text{ m}$ , and  $h = 0.008 \text{ m}$  throughout our simulations. All composite plates are made of Boron/Aluminum metal matrix composites with

elastic properties obtained through a micromechanical analysis of periodically heterogeneous anisotropic materials [34] and coefficients of thermal expansion obtained from micromechanical formulations provided in [27]:  $E_1 = 215.3$  GPa,  $E_2 = E_3 = 144.1$  GPa,  $G_{12} = G_{13} = 54.39$  GPa,  $G_{23} = 45.92$  GPa,  $\nu_{12} = \nu_{13} = 0.195$ ,  $\nu_{23} = 0.255$ ,  $\rho = 2653$  kg/m<sup>3</sup>,  $\alpha_{11} = 10.615 \times 10^{-6}/^\circ\text{C}$ , and  $\alpha_{22} = 15.997 \times 10^{-6}/^\circ\text{C}$ . FEA uses the ANSYS SHELL99 multilayered 8-noded shell element with  $60 \times 20$  elements. Using  $m \times n$  to denote the mode shape of  $w = W_{mn} \sin(m\pi x_1) \sin(n\pi x_2/r)$ , 27 modes,  $(1, 2, 3, 4, 5, 6, 7, 8, 9) \times (1, 2, 3)$ , are used in the analytical method throughout the rest of analysis. The compressive load and temperature under analysis is increased quasi-statically and the temperature distribution takes the form of  $\Delta T(x_3) = \Delta T_0 + T_1 x_3$ .

The comparison between analytical and FEA methods on linear buckling loads for antisymmetric angle-ply composite laminates is shown in table 1. Results for antisymmetric cross-ply are not included, because plates with such laminate configuration typically demonstrate a prebuckling deformation behavior, therefore, prevent the occurrence of pitchfork bifurcations. The present method matches well with FEA in predicting first six linear buckling loads (for pure mechanical buckling case) and linear buckling temperatures (for thermal buckling case). Further validation of the present method is provided in Fig. 3, where the

Table 1

Linear buckling comparison between analytical and FEA methods for antisymmetric angle-ply composite laminates

Mechanical buckling (Case 1)				Thermal buckling <sup>a</sup> (Case 2)			
Buckling load	Analytical $\times 10^5$ N/m	ANSYS $\times 10^5$ N/m	Buckling mode	Buckling temperature	Analytical $^\circ\text{C}$	ANSYS $^\circ\text{C}$	Buckling mode <sup>b</sup>
$\bar{N}_{11cr1}$	5.96837	5.96225	(2, 1)	$\Delta T_{cr1}$	11.300	11.308	(1, 1)
$\bar{N}_{11cr2}$	6.14117	6.13671	(1, 1)	$\Delta T_{cr2}$	15.760	15.776	(2, 1)
$\bar{N}_{11cr3}$	6.90244	6.89213	(3, 1)	$\Delta T_{cr3}$	22.646	22.680	(3, 1)
$\bar{N}_{11cr4}$	8.63853	8.62019	(4, 1)	$\Delta T_{cr4}$	31.926	31.994	(4, 1)
$\bar{N}_{11cr5}$	11.1032	10.9997	(5, 1)	$\Delta T_{cr5}$	40.260	40.369	(1, 2)
$\bar{N}_{11cr6}$	14.0270	13.9728	(6, 1)	$\Delta T_{cr6}$	43.639	43.766	(5, 1)

<sup>a</sup> Thermal buckling results in this table is obtained by assuming a uniformly distributed temperature field, i. e.,  $\Delta T = \Delta T_0$ .

<sup>b</sup>  $(m, n)$  denotes mode shape of  $A_{mn} \sin(m\pi x_1) \sin(n\pi x_2/r)$ .

postbuckling temperature-deflection curves of an imperfect angle-ply laminated plate (with initial central deformation being 2% of the thickness introduced by a uniformly distributed pressure  $f_3 = 845.721$  N/m<sup>2</sup>) and a perfect cross-ply laminated plate are compared with results obtained by ANSYS. It is evident that good agreement is achieved in this comparison study. Moreover, although in both cases the analysis using ANSYS fails to converge when temperature rises close to the secondary buckling value, the analytical approach, as will be shown latter, can go far beyond the secondary bifurcation point and pass through multiple unstable equilibrium branches and bifurcation points to capture the mode jumping phenomenon.

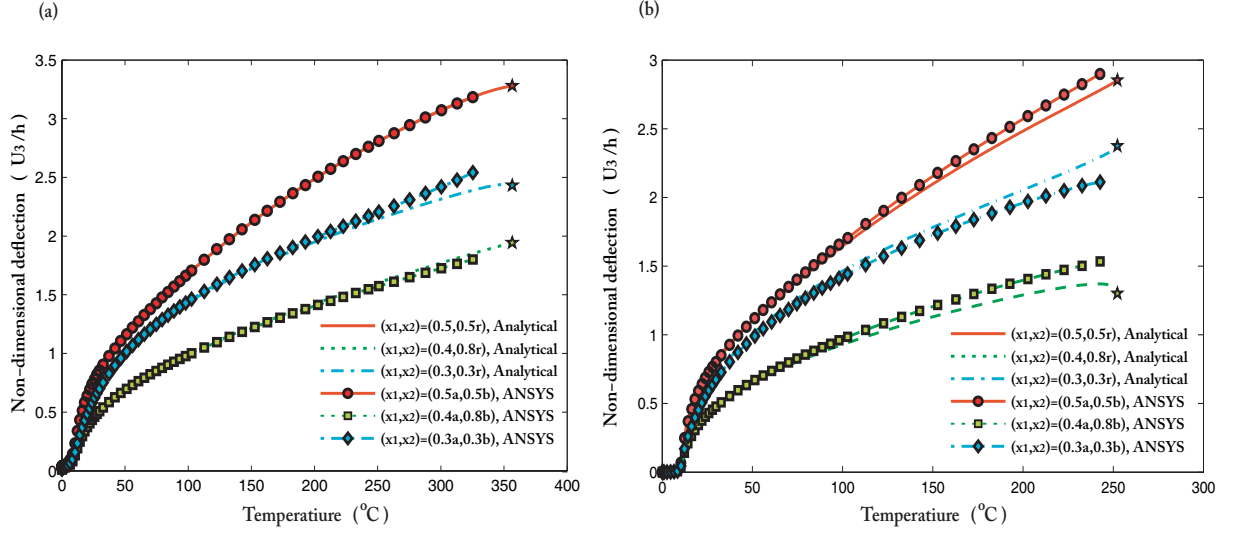


Fig. 3. Comparison of postbuckling equilibria for thermally buckled angle-ply and cross-ply laminates. (a) angle-ply laminated plate (case 2) with 2% initial imperfection ( $U_3(a/2, b/2) = 0.02h$ ) generated by vertical pressure  $f_3 = 845.7206 \text{ N/m}^2$ ; (b) perfect cross-ply laminated plate (case 3). Symbol star denotes the secondary bifurcation points

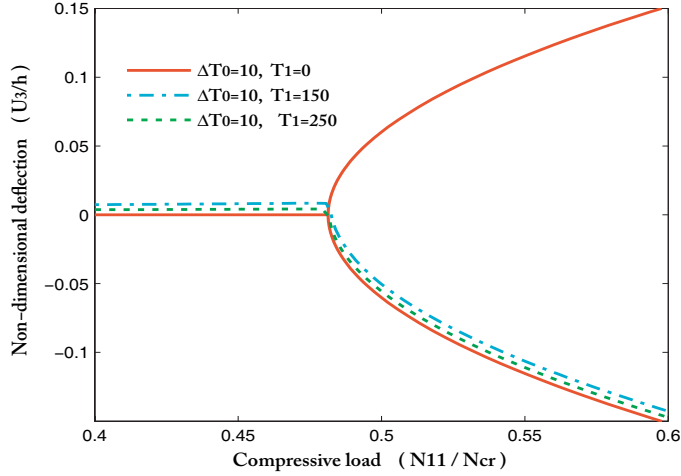


Fig. 4. Central deflection versus compressive load under the effect of different temperature distributions, case 1.  $N_{cr}$  is the critical buckling load of this plate with no thermal effect.

Table 2

The variation of thermomechanical buckling load with specified temperature  $\Delta T_0$  for antisymmetric angle-ply laminated plate, case 1,  $T_1 = 0$ .

$\Delta T_0$	$0^{\circ}\text{C}$	$5^{\circ}\text{C}$	$10^{\circ}\text{C}$	$15^{\circ}\text{C}$	$20^{\circ}\text{C}$	$30^{\circ}\text{C}$	$40^{\circ}\text{C}$
$\bar{N}_{11cr1} \times 10^5 \text{ N/m}$	5.9837	4.5018	2.8732	1.2392	-3.9477	-3.6627	-5.1285
Buckling mode	(2, 1)	(1, 1)	(1, 1)	(1, 1)	(1, 1)	(1, 1)	(2, 1)

The effects of constant temperature raising ( $\Delta T_0$ ) and temperature gradient ( $T_1$ ) on linear critical buckling load ( $N_{11cr1}$ ) and postbuckling equilibrium paths for a thermomechanically stressed angle-ply laminated plate (case 1) are illustrated in table 2 and Fig. 4. The increase of temperature  $\Delta T_0$  will induce a drop of critical buckling load and provoke a change of

buckling mode when temperature reaches certain values. As the buckling temperature for this plate under pure thermal loading is  $\Delta T_0 = 18.778^\circ\text{C}$ , it is no surprise to find that the critical buckling load will change its sign when  $\Delta T_0$  increases above  $20^\circ\text{C}$ , indicating the necessity of applying a minimum amount of tensional force to keep the plate flat. Setting  $T_1 = 150$  or  $250^\circ\text{C}/\text{m}$  will generate a small amount of the temperature discrepancy between the top and bottom of the laminated plate, i.e.,  $T_{top} - T_{bot} = T_1 h = 1$  or  $2^\circ\text{C}$ , leading to the breaking of the pitchfork bifurcation structure. Therefore, the effect generated by temperature gradient is similar to that introduced by initial geometric imperfections.

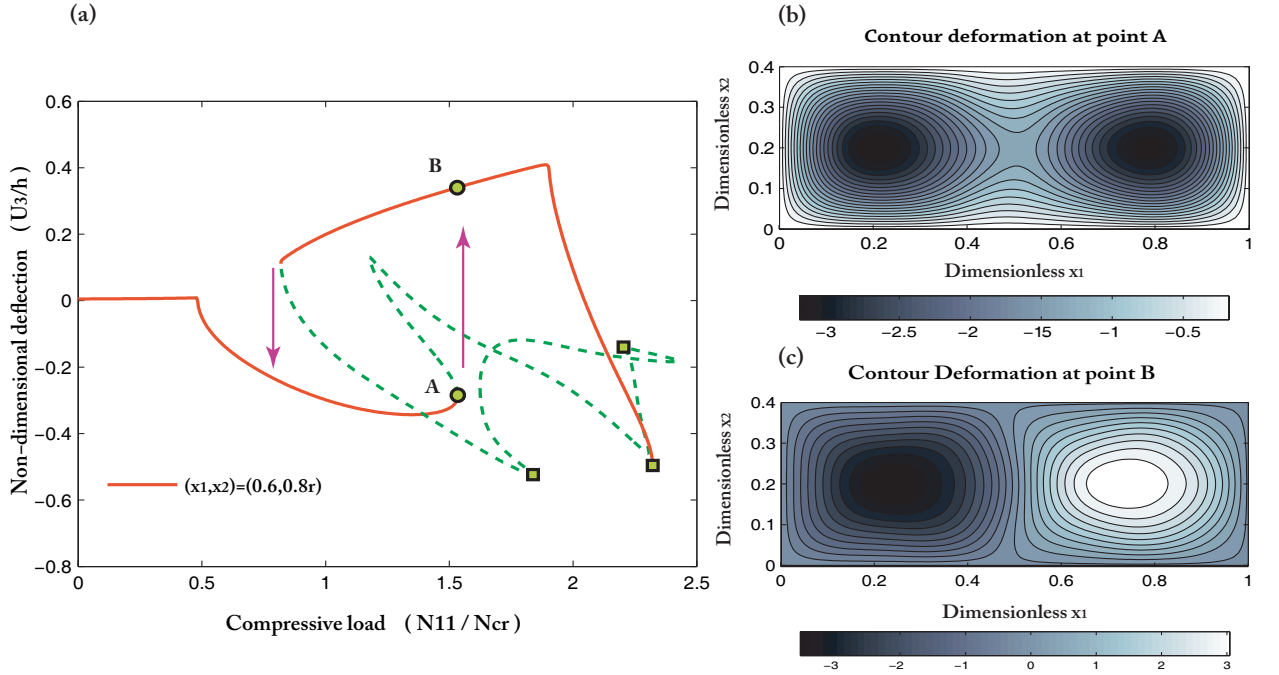


Fig. 5. Bifurcation diagram and static deformation patterns at representing points for thermomechanically buckled perfect angle-ply laminate, case 1 ( $\Delta T_0 = 10^\circ\text{C}$ ,  $T_1 h = 2^\circ\text{C}$ ). (a) bifurcation diagram; (b) and (c) buckling patterns at the secondary buckling load for points A and B. Stable paths are shown as solid lines and unstable paths as broken lines. Square symbols represents bifurcation points.

The secondary instability and mode jumping behavior of the plate model analyzed in Fig. 4 is further illustrated in Fig. 5. The plate is subjected to the combination of uniaxially compressive load  $\bar{N}_{11}$  and a temperature field with  $\Delta T_0 = 10^\circ\text{C}$  and  $T_1 = 250^\circ\text{C}/\text{m}$ . Clearly, the first bifurcation occurs at  $N_{11}/N_{cr} = 0.48$  and the second at  $N_{11}/N_{cr} = 1.53$ . The introduced constant temperature increase  $\Delta T_0$  reduces the critical buckling load to 1/2 of its original value ( $\Delta T_0 = 0$ ) while the temperature gradient  $T_1$  induces a thermal imperfection and annihilate the primary bifurcation point and changes the secondary bifurcation point to a limit point. When compared with the “exact” secondary bifurcation results obtained without any mechanical or thermal imperfections (not shown here), this imperfect plate only generates a small amount change in its first and second buckling locations. Mode jumping occurs at the secondary buckling point where the primary postbuckling branch loses its stability and the laminated plate will jump from its current stable configuration (point A) to a remote stable configuration (point B). The plate experiences a smooth propagation of its buckling pattern along the primary postbuckling branch until the secondary buckling point is reached,

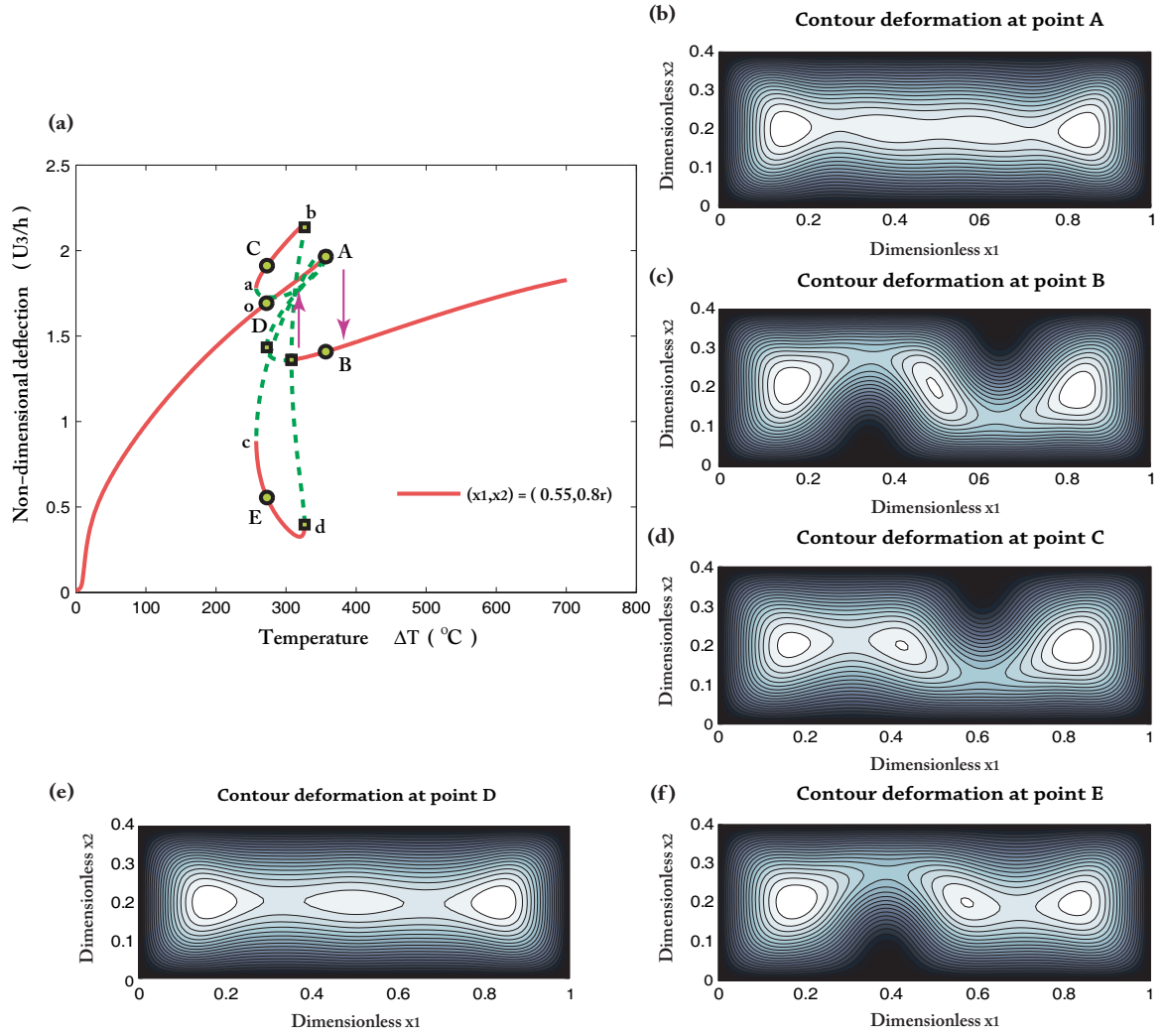


Fig. 6. Bifurcation diagram and static deformation patterns at representing points for thermally buckled imperfect angle-ply laminate, case 2 ( $f_3 = 845.721\text{N/m}^2$ ,  $w_c = 0.02h$ ,  $T_1h = 0^\circ\text{C}$ ). (a) bifurcation diagram; (b) ~ (f) buckling patterns for representing points A ~ E. Stable paths are shown as solid lines and unstable paths as broken lines. Square symbols represents bifurcation points.

indicating a change of wave numbers of the buckling pattern in compressive load direction. The hysterical behavior in Fig. 5 suggests that the plate jumps back from the remote stable path to the primary postbuckling path during an unloading process.

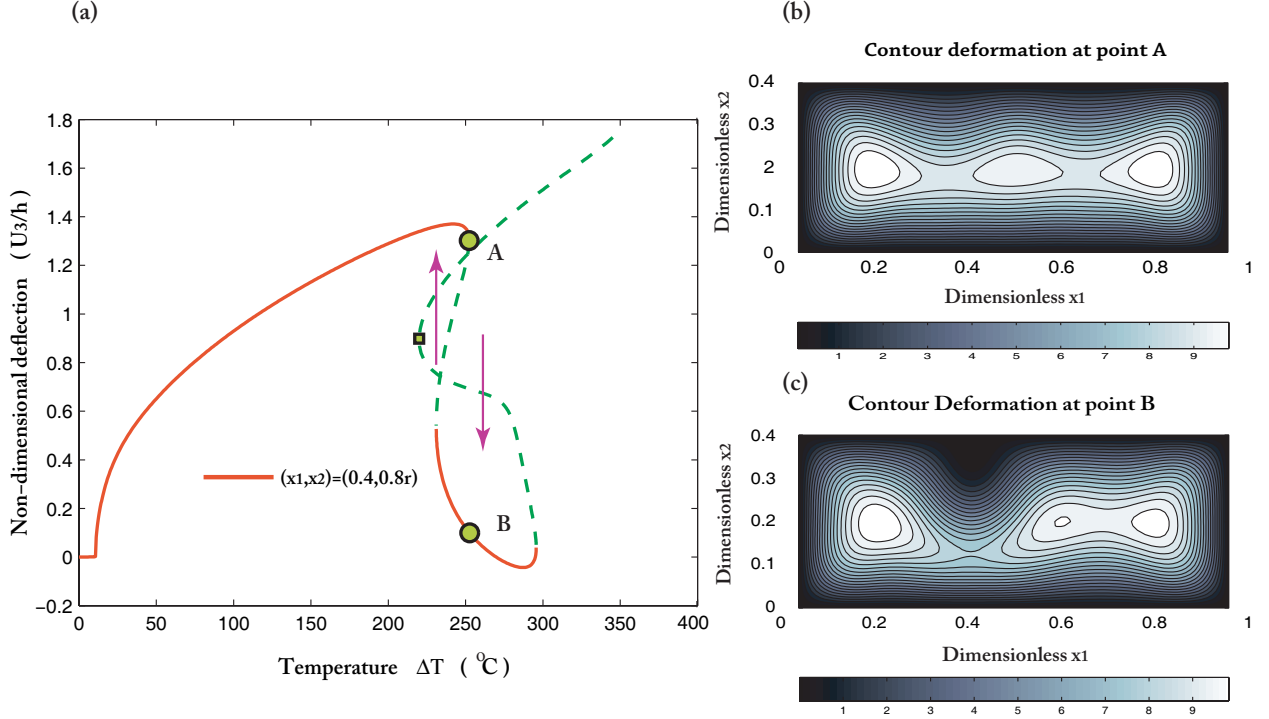


Fig. 7. Bifurcation diagram and static deformation patterns at representing points for thermally buckled perfect cross-ply laminate, case 3 ( $T_1 h = 0^\circ\text{C}$ ). (a) bifurcation diagram; (b) and (c) buckling patterns at secondary buckling temperature for points A and B. Stable paths are shown as solid lines and unstable paths as broken lines. Square symbols represents bifurcation points.

Fig. 6 reveals the mode jumping behavior of a thermally stressed angle-ply plate with four straight edges constrained in plane (case 2). The plate is subjected to a uniformly distributed temperature field  $\Delta T_0$  and a vertical pressure  $f_3 = 845.721\text{N/m}^2$  is added in analysis to introduce an initial imperfection with maximum out-of-plane deflection up to 2% of the plate thickness. Although the primary buckling temperature for the perfect plate ( $f_3 = 0$ ) is  $\Delta T_{0cr1} = 11.308^\circ\text{C}$ , the secondary bifurcation occurs at  $\Delta T_{0cr2} = 356.5^\circ\text{C}$  with  $\Delta T_{0cr2}/\Delta T_{0cr1} = 31.5$ , far deep into the postbuckling range. This is due to that the thermally loaded plate demonstrates much stronger geometrical nonlinearity caused by the extensive coupling between the out-of-plane deformation and boundary constraints than its mechanically-loaded counterparts [6]. When temperature is increased beyond the secondary bifurcation load, the plate exhibits a subcritical bifurcation behavior, indicated by the symmetry of unstable equilibrium paths near the secondary bifurcation point. In addition, the plate experiences a significant change of its buckling pattern— from a symmetric pattern (with respect to both  $x_1$  and  $x_2$  axes) at point A to an asymmetric one at point B. The co-existence of multiple stable branches (ab, oA, and cd) is also observed in this figure.

Static deformation patterns at points C, D, E ( $\Delta T_0 = 272.6^\circ\text{C}$ ) on these stable branches are given in Figs. 6 (d), (e), and (f). It is interesting to note that although the buckling pattern at point D on the primary stable postbuckling branch displays a symmetry with respect to  $x_1$  and  $x_2$  axes, the buckling patterns at C and E are asymmetric and they demonstrate an antisymmetric relationship with each other with respect to the center of the plate—buckling pattern at point C seems can be obtained by two successive flips of the buckling pattern at point E. The exhibition of certain kind symmetric relationship between the buckling patterns on the remote stable branch pair is not uncommon, as it has been frequently observed in many investigations on mode jumping of both isotropic and composite plates [6,7,15].

The thermal postbuckling and mode jumping of a perfect cross-ply laminate with four edges fixed in-plane (case 3) are depicted in Fig. 7. The plate is subjected to uniformly distributed temperature field  $\Delta T_0$ . In spite of the fact that no pitchfork bifurcation exists for cross-ply plate, the plate demonstrates a rapid increase of out-of-plane deformation at  $\Delta T_0 = 10.67^\circ\text{C}$ , indicating the effect of a ‘nominal’ primary bifurcation point which can be calculated by ignoring the prebuckling terms in Eq. (52). The secondary instability again happens far deep into the postbuckling range,  $\Delta T_0 = 253.3^\circ\text{C}$  and  $\Delta T_{0cr2}/\Delta T_{0cr1} = 23.65$ . The significant change of buckling patterns before and after mode jumping is observed in Figs. 7 (b) and (c).

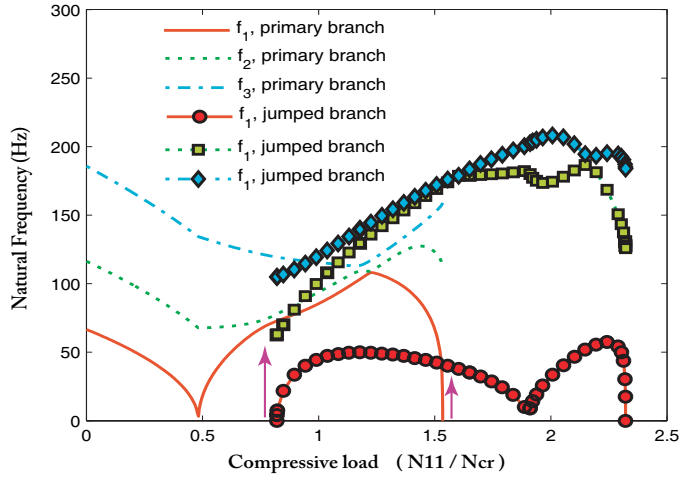


Fig. 8. Natural frequencies versus compressive load for thermomechanically buckled perfect angle-ply plate, case 1 ( $\Delta T_0 = 10^\circ\text{C}$ ,  $T_1 h = 2^\circ\text{C}$ ).

#### 4.2 Dynamic analysis

Figs. 8, 9, and 10 delineate the variation of the lowest three natural frequencies as a function of compressive load/temperature for three plate models analyzed in Figs. 5, 6, and 7, as we trace the stable equilibrium paths before and after the snapping. The fundamental natural frequency drops to zero at bifurcation points or limit points, designating the stiffness matrix becoming singular at these points. Mode jumping is always accompanied by a leap in fundamental frequency. For example, in Fig. 8, dramatic increments of fundamental frequency from zero to 41.5 Hz at  $N_{11}/N_{11cr} = 1.53$  and 76.2 Hz at  $N_{11}/N_{11cr} = 0.82$  are observed during the loading and unloading processes, respectively. Similar leaps can

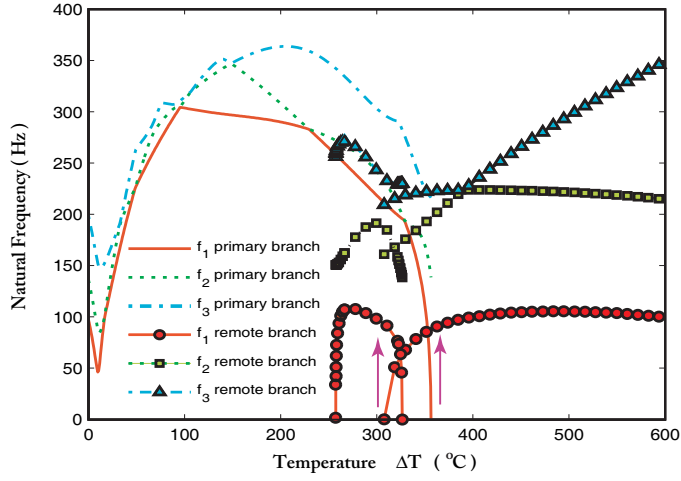


Fig. 9. Natural frequencies versus temperature  $\Delta T_0$  for thermally buckled imperfect angle-ply plate, case 2 ( $f_3 = 845.721\text{N/m}^2$ ,  $w_c = 0.02h$ ,  $T_1h = 0^\circ\text{C}$ ).

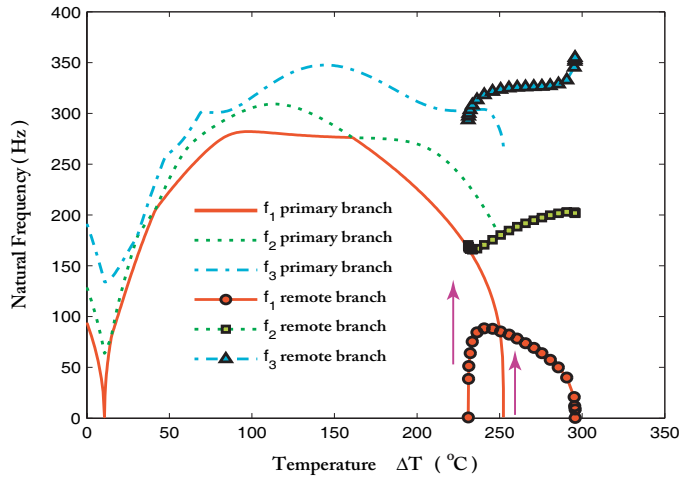


Fig. 10. Natural frequencies versus temperature  $\Delta T_0$  for thermally buckled perfect cross-ply plate, case 3 ( $T_1h = 0^\circ\text{C}$ ).

also be found in Fig. 9 and 10. A careful observation of Fig. 8 shows the occurrence of a ‘modal shifting’ phenomenon at a point in the primary postbuckling regime when  $N_{11}/N_{11cr} = 1.23$ , where the fundamental frequency curve intersects the second natural frequency curve and the fundamental vibration mode shapes changes to the second vibration mode shape as  $N_{11}/N_{11cr}$  increases beyond 1.23. In Fig. 9, the ‘modal shifting’ occurs at  $\Delta T_0 = 16.59^\circ\text{C}$ ,  $47.39^\circ\text{C}$ ,  $95.3^\circ\text{C}$ ,  $229.2^\circ\text{C}$ , and  $329.2^\circ\text{C}$ , while in Fig. 10, this phenomenon is observed at  $\Delta T_0 = 14.82^\circ\text{C}$ ,  $41.98^\circ\text{C}$ , and  $160.8^\circ\text{C}$ . Another interesting phenomenon observed is how natural frequencies varies along the pair of co-existent stable remote branches (segments ab and cd in Fig. 6). Fig. 9 indicates that the first three natural frequencies pairs obtained by tracing along the two stable equilibrium paths are identical with respect to each other. This is consistent with previous static observations of the demonstration of symmetry between buckling patterns along the co-existed remote stable branch pair.

## 5 Concluding remarks

This paper presents a rigorous analytic method to study the secondary instability (bifurcation) and mode jumping of simply-supported antisymmetric angle-ply and cross-ply laminated plates subjected to thermomechanical loadings. Unlike most existing approaches in the literature, kinematic relations and dynamic governing PDEs of composite plates are derived rigorously from the variational asymptotic theory, which reduces the formulation of the 3-D elastic problem to that of its 2-D counterpart. The carefully selected nondimensionalization scheme generates well proposed PDEs suitable for bifurcation analysis. A novel and simpler solution procedure is developed to solve the two coupled compatibility and governing equations. The compact and explicit transformation of nonlinear PDEs to a system of nonlinear ODEs enables a systematic investigation of effects of multi-mode interactions on postbuckling response and the snapping phenomenon. Generalized Galerkin method is used to solve the boundary value problems for antisymmetric angle-ply and cross-ply laminated plates. Because the present method involves the most generalized solution procedure to handle various boundary effects, it can be readily extended to analyze simply-supported composite plates with arbitrary lamination configurations.

The comparisons between the present method and FEA demonstrate a good agreement in their numerical results in the primary postbuckling region. While FEA loses its convergence when solution comes close the secondary bifurcation point, the present method has the capability of exploring deeply into the post-secondary buckling realm and capture the mode jumping phenomenon for various combinations of plate configurations boundary conditions. Various postbuckling patterns of different complexity are found before and after the mode jumping. Natural frequencies of composite plates are calculated along the stable primary postbuckling and the jumped equilibrium paths. The exchange of vibration modal shape or 'modal shifting' phenomenon is found for different plate models under consideration.

## Acknowledgements

This study is partially supported by the National Science Foundation under Grant DMI-0522908 and the Space Dynamics Laboratory at the Utah State University under Shunk Works Grant. The views and findings contained herein are those of the authors and should not be interpreted as necessarily representing the official policies or endorsement, either expressed or implied, of the funding agencies.

## Appendix A. Coefficients for angle-ply and cross-ply laminated plates

The coefficients, vectors, and matrices needed in dynamic equation Eq. (43) for antisymmetric angle-ply laminates are:

$$V_{1x} = \left\{ \begin{array}{l} \frac{1}{2}, \text{ if } p = k + m; \text{ else } 0 \\ \pm \frac{1}{2}, \text{ if } p = \pm(k - m); \text{ else } 0 \end{array} \right\}, \quad V_{1y} = \left\{ \begin{array}{l} \frac{1}{2}, \text{ if } q = l + n; \text{ else } 0 \\ \pm \frac{1}{2}, \text{ if } q = \pm(l - n); \text{ else } 0 \end{array} \right\}, \quad (\text{A-1})$$

$$L_1 = (2\tilde{B}_{26} - \tilde{B}_{61})r^2 \begin{bmatrix} (k+m)^3(l+n)c_1 & (k+m)^3(l-n)c_2 \\ (k-m)^3(l+n)c_3 & (k-m)^3(l-n)c_4 \end{bmatrix} \quad (\text{A-2})$$

$$+ (2\tilde{B}_{16} - \tilde{B}_{62}) \begin{bmatrix} (k+m)(l+n)^3c_1 & (k+m)(l-n)^3c_2 \\ (k-m)(l+n)^3c_3 & (k-m)(l-n)^3c_4 \end{bmatrix},$$

$$V_{2x} = \begin{pmatrix} \frac{1}{2}, & \text{if } p = i + k + m; & \text{else } 0 \\ \pm\frac{1}{2}, & \text{if } p = \pm(i + k - m); & \text{else } 0 \\ \pm\frac{1}{2}, & \text{if } p = \pm(i - k - m); & \text{else } 0 \\ \pm\frac{1}{2}, & \text{if } p = \pm(i - k + m); & \text{else } 0 \end{pmatrix}, \quad V_{2y} = \begin{pmatrix} \frac{1}{2}, & \text{if } q = j + l + n; & \text{else } 0 \\ \pm\frac{1}{2}, & \text{if } q = \pm(j + l - n); & \text{else } 0 \\ \pm\frac{1}{2}, & \text{if } q = \pm(j - l - n); & \text{else } 0 \\ \pm\frac{1}{2}, & \text{if } q = \pm(j - l + n); & \text{else } 0 \end{pmatrix}, \quad (\text{A-3})$$

$$g(\Delta T) = \begin{cases} \frac{16\mathfrak{M}_{T11}p}{q}, & \text{if } p \text{ even and } q \text{ odd,} \\ \frac{16\mathfrak{M}_{T22}q}{pr^2}, & \text{if } p \text{ odd and } q \text{ even,} \\ 0, & \text{else.} \end{cases} \quad G_1 = \begin{bmatrix} (kn - lm)^2 & (kn + lm)^2 \\ (kn + lm)^2 & (kn - lm)^2 \end{bmatrix}, \quad E = \begin{bmatrix} E_{11} & E_{12} \\ E_{12} & E_{11} \end{bmatrix}, \quad (\text{A-4})$$

$$E_{11} = \begin{bmatrix} [(k+m)j - (l+n)i]^2 c_1 & [(k+m)j - (l-n)i]^2 c_2 \\ [(k-m)j - (l+n)i]^2 c_3 & [(k-m)j - (l-n)i]^2 c_4 \end{bmatrix}, \quad (\text{A-5})$$

$$E_{12} = \begin{bmatrix} [(k+m)j + (l+n)i]^2 c_1 & [(k+m)j + (l-n)i]^2 c_2 \\ [(k-m)j + (l+n)i]^2 c_3 & [(k-m)j + (l-n)i]^2 c_4 \end{bmatrix}. \quad (\text{A-6})$$

The coefficients, vectors, and matrices needed in dynamic equation Eq. (52) for antisymmetric cross-ply laminates are:

$$\begin{cases} C_{B1} = \frac{4pr}{q}\tilde{B}_{11}, \quad C_{B2} = \frac{4pr}{q}\tilde{B}_{21} & \text{if } p \text{ even and } q \text{ odd,} \\ C_{B1} = \frac{4q}{pr}\tilde{B}_{12}, \quad C_{B2} = \frac{4q}{pr}\tilde{B}_{22} & \text{if } p \text{ odd and } q \text{ even,} \\ C_{B1} = 0, \quad C_{B2} = 0 & \text{else,} \end{cases} \quad (\text{A-7})$$

$$\begin{cases} C_{L3} = \frac{\pi^2 pr}{8}, \quad L_3 = \tilde{B}_{11}L_{31} + \tilde{B}_{21}r^2L_{32} & \text{if } p + k + m \text{ even and } q + l + n \text{ odd,} \\ C_{L3} = \frac{\pi^2 q}{8r}, \quad L_3 = \tilde{B}_{12}L_{31} + \tilde{B}_{22}r^2L_{32} & \text{if } p + k + m \text{ odd and } q + l + n \text{ even,} \\ C_{L3} = 0, \quad L_3 = 0 & \text{else,} \end{cases} \quad (\text{A-8})$$

$$\begin{cases} V_{3x} = V_{4x} = \left\{ \frac{4p}{p^2 - (k+m)^2}, \frac{4p}{p^2 - (k-m)^2} \right\}^T, & \text{if } p+k+m \text{ odd} \\ V_{3x} = \{0, 0\}^T, V_{4x} = \{2, 2\}^T, & \text{if } p+k+m \text{ even} \end{cases} \quad (\text{A-9})$$

$$\begin{cases} V_{3y} = V_{4y} = \left\{ \frac{4q}{q^2 - (l+n)^2}, \frac{4q}{q^2 - (l-n)^2} \right\}^T, & \text{if } q+l+n \text{ odd} \\ V_{3y} = \{0, 0\}^T, V_{4y} = \{2, 2\}^T & \text{if } q+l+n \text{ even} \end{cases} \quad (\text{A-10})$$

$$\begin{aligned} L_2 = & \tilde{B}_{21} r^4 \begin{bmatrix} (k+m)^4 c_1 & (k+m)^4 c_2 \\ (k-m)^4 c_3 & (k-m)^4 c_4 \end{bmatrix} + (\tilde{B}_{11} + \tilde{B}_{22}) r^2 \\ & \begin{bmatrix} (k+m)^2 (l+n)^2 c_1 & (k+m)^2 (l-n)^2 c_2 \\ (k-m)^2 (l+n)^2 c_3 & (k-m)^2 (l-n)^2 c_4 \end{bmatrix} + \tilde{B}_{12} \begin{bmatrix} (l+n)^4 c_1 & (l-n)^4 c_2 \\ (l+n)^4 c_3 & (l-n)^4 c_4 \end{bmatrix} \end{aligned} \quad (\text{A-11})$$

$$G_2 = \begin{bmatrix} (kn - lm)^2 - (kn + lm)^2 \\ -(kn + lm)^2 (kn - lm)^2 \end{bmatrix}, L_{31} = \begin{bmatrix} (l+n)^2 c_1 (l-n)^2 c_2 \\ (l+n)^2 c_3 (l-n)^2 c_4 \end{bmatrix}, L_{32} = \begin{bmatrix} (k+m)^2 c_1 (k+m)^2 c_2 \\ (k-m)^2 c_3 (k-m)^2 c_4 \end{bmatrix}, \quad (\text{A-12})$$

## References

- [1] M. Stein. Loads and deformation of buckled rectangular plates. NASA Technical Report R-40, National Aeronautics and Space Administration, 1959.
- [2] T. Nachiketa. Secondary buckling of compression-loaded composite plates. *AIAA Journal*, 40(10):2120–2126, 2002.
- [3] B. Audoly, B. Roman, and A. Pocheau. Secondary buckling patterns of thin plate under in-plane compression. *The European Physical Journal*, 27:7–10, 2002.
- [4] M. George, C. Coupeau, J. Colin, F. Cleymand, and J. Grilhe. Delamination of metal thin films on polymer substrates: from streight-side blisters to varicose structures. *Philosophical Magazine A*, 82:633– 641, 2002.
- [5] N. Sridhar, D. J. Srolovitz, and B. N. Cox. Buckling and post-buckling kenetics of compressed thin films on viscous subtrates. *Acta Materialia*, 50:2547–2557, 2002.
- [6] H. Chen and L. N. Virgin. Dynamic analysis of modal shifting and mode jumping in thermally buckled plates. *Journal of Sound and Vibration*, 278:233 – 256, 2004.
- [7] H. Chen and L. N. Virgin. Finite element analysis of post-buckling dynamics in plates. part i: An asymptotic approach. *International Journal of Solids and Structures*, 43(13):3983–4007, 2006.
- [8] B. G. Falzon and G. P. Steven. Buckling mode transition in hat-stiffened composite panels loaded in uniaxial compression. *Composite Structures*, 37(2):253– 267, 1997.

- [9] D. W. Jensen and P. A. Lagace. Influence of mechanical couplings on the buckling and post-buckling of anisotropic plates. *AIAA Journal*, 26(10):1269–1277, 1998.
- [10] A. C. Orifici, R. S. Thomson, A. J. Gunnion, R. Degenhardt, H. Abramovich, and J. Bayandor. Benchmark finite element simulations of postbuckling composite stiffened panels. In *Proceedings of the 11th Australian International Aerospace Congress*, Melbourne, Australia, March 2005.
- [11] D. J. Dawe and S. Wang. Postbuckling analysis of composite laminated panels. *AIAA Journal*, 38(11):2160–2170, 2000.
- [12] B. G. Falzon and M. Cerini. An automated hybrid procedure for capturing mode-jumping in postbuckling composite structures. *Composite Structures*, 73:186–195, 2006.
- [13] E. Riks, C. C. Rankin, and F. A. Brogan. On the solution of mode jumping phenomena in thin-walled shell structures. *Computer Methods in Applied Mechanics and Engineering*, 136:59–92, 1996.
- [14] H. Chen and L. N. Virgin. Finite element analysis of post-buckling dynamics in plates. part ii: A non-stationary analysis. *International Journal of Solids and Structures*, 43(13):4008–4027, 2006.
- [15] H. Chen and W. Yu. Postbuckling and mode jumping analysis of composite laminates using an asymptotically correct, geometrical nonlinear theory. *International Journal of nonlinear mechanics*, submitted 2006.
- [16] H.-S. Shen. Thermal postbuckling of preloaded shear deformable laminated plates. *Journal of Engineering Mechanics*, 126(5):488–496, 2000.
- [17] J. B. Dafedar and Y. M. Desai. Thermomechanical buckling of laminated composite plates using mixed, higher-order analytical formulation. *Journal of Applied Mechanics*, 69:790–799, 2002.
- [18] L. Yang K. M. Liew and S. Kitipornchai. Thermal postbuckling of laminated plates comprising functionally graded materials with temperature-dependent properties. *Journal of Applied Mechanics*, 71:839–850, 2004.
- [19] J.-H. Roh, I.-K. Oh, S.-M. Yang, J.-H. Han, and I. Lee. Thermal post-buckling analysis of shape memory alloy hybrid composite shell panels. *Smart Materials and Structures*, 13:1337–1344, 2004.
- [20] A. K. Noor and S. W. Burton. Assessment of shear deformation theories for multilayered composite plates. *Applied Mechanics Review*, 41(1):1–13, 1989.
- [21] A. K. Noor and S. W. Burton. Assessment of computational models for multilayered composite shells. *Applied Mechanics Review*, 43(4), April 1990.
- [22] A. K. Noor and M. Malik. An assessment of five modeling approaches for thermo-mechanical stress analysis of laminated composite panels. *Computational Mechanics*, 25:43–58, 2000.
- [23] J. N. Reddy. A simple higher-order theory for laminated composite plates. *Journal of Applied Mechanics*, 51:745–752, 1984.
- [24] M. Touratier. An efficient standard plate theory. *International Journal of Engineering Science*, 29:901–916, 1991.

- [25] M. DiSciuva. Development of anisotropic multilayered shear deformable rectangular plate element. *Computers and Structures*, 21:789 – 796, 1985.
- [26] Y. B. Cho and R. C. Averill. First-order zig-zag sublaminated plate theory and finite element model for laminated composite and sandwich panels. *Composite Structures*, 50:1 – 15, 2000.
- [27] J. N. Reddy. *Mechanics of Laminated Composite Plates and Shells, Theory and Analysis*. CRC Press, second edition, 2004.
- [28] W. Yu and D. H. Hodges. Asymptotic approach for thermoelastic analysis of laminated composite plates. *Journal of Engineering Mechanics*, 130(5):531– 540, 2004.
- [29] V. L. Berdichevsky. Variational-asymptotic method of constructing a theory of shells. *PMM*, 43(4):664 – 687, 1979.
- [30] W. Yu, D. H. Hodges, and V. V. Volovoi. Asymptotic construction of Reissner– like composite plate theory with accurate strain recovery. *International Journal of Solids and Structures*, 39:5185 – 5203, 2002.
- [31] D. H. Hodges, A. R. Atilgan, and D. A. Danielson. A geometrically nonlinear theory of elastic plates. *Journal of Applied Mechanics*, 60(1):109 – 116, March 1993.
- [32] D. H. Hodges, W. Yu, and M. Patil. Geometrically-exact, intrinsic theory for dynamics of moving composite plates. In *Proceedings of the 47th Structures, Structural Dynamics and Materials Conference*, Newport, Rhode Island, May 1 – 4 2006. AIAA.
- [33] E. H. Doedel, A. R. Champneys, T. F. Fairgrieve, Y. A. Kuznetsov, B. Sandstede, and X.-J. Wang. Auto 97: Continuation and bifurcation software for ordinary differential equations. Technical Report, Department of Computer Science, Concordia University, Montreal, Canada, 1997.
- [34] W. Yu and T. Tang. Asymptotical construction of a micromechanics model for periodically heterogeneous anisotropic materials. In *Proceedings of the 47th Structures, Structural Dynamics, and Materials Conference*, Newport, Rhode Island, May 2006.